Wide field polarization calibration in the image plane using the Allen Telescope Array

Mattieu de Villiers, SKA SA
Casey Law, UC Berkeley

28 October 2010

Abstract

This study investigates wide field polarization calibration using the Allen Telescope Array (ATA) for the purpose of correcting errors in the imaged Stokes I, Q, U, V parameters that are due to primary beam effects. It is shown that the overall direction dependent polarimetric response of the interferometer can be determined from visibility data of pointings in the vicinity of the well known stable linearly polarized calibrator 3C 286. The polarimetric response is encapsulated by seven independent components of a Mueller matrix that relate to leakage and gain errors. In the case of the ATA these components can be modeled effectively using quadratics over the part of the primary beam that extends to half the distance to the half power point. If the model, which is fixed in primary beam coordinates, is applied to the ATA data knowing the parallactic angles and offset positions, then an improvement is noted in RMS errors of the imaged Stokes Q and U values from around 0.9 % down to 0.2 % with respect to the true Stokes I over the part of the field considered.

1 Introduction

Traditionally, calibration is only performed at the pointing center with the consequence that the correctness in polarization of resulting images degrades further across the field. Normalization by the primary beam power pattern post imaging may adequately correct the intensity roll-off in total intensity imaging under some conditions. However such simple normalization does not correct position angle errors. In fact, direction dependent effects in the context of polarization have largely been overlooked until recently.

When the full co and cross polarization antenna primary beam patterns are accurately known, equivalent convolution kernels can be derived and applied in the visibility domain during gridding to account for direction dependent effects [Bhatnagar: 2008]. Under this condition, some success in extracting pointing errors from observations has been reported. However, little work has yet been done to infer a primary beam model itself from astronomical observations. This memo reports on a wide field polarization calibration study which explores this area using the ATA.

Since Miriad is entirely integrated into the ATA, all development is done on top of Miriad tools. A previous study [Law: 2010] investigates the way by which calibration leakage solutions change due to wide field and wide bandwidth effects. It was found that calibration solutions with effective polarization leakages of up to 50% are computed when calibrating for off-center pointings as far away as half the distance to the half power point of the primary beam.

The Miriad calibration algorithm assumes small leakages and sometimes fails to determine solutions in such cases. This problem is circumvented by a two stage calibration approach where on-center calibration is first done using a known calibrator in the center of the field in

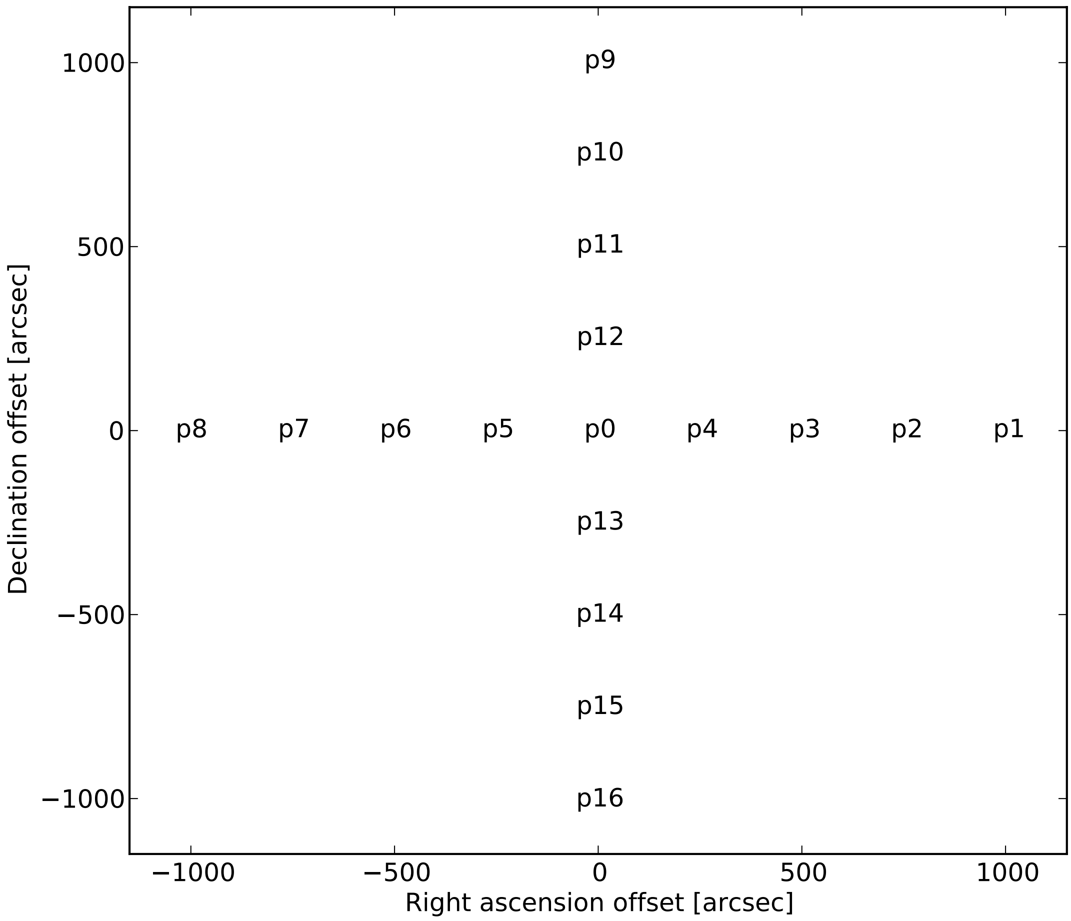

Figure 1: Pointings in the cross 17 dataset.

the usual way. The direction dependent effects are then explored using off-center pointings of the same calibrator subject to the original calibration.

Results show that the polarimetric response of the ATA can be modeled using a simple quadratic over a part of the field of view that extends to half the distance to the half power point. Errors in the imaged Stokes I,Q,U,V are illustrated in the Results section for the case when no direction dependent corrections are made, and also for the case when corrections are made using the inferred model.

The end goal of this study is to devise a practical calibration strategy for the ATA that effectively deals with wide field and wide bandwidth effects. Although this memo shows that a simple quadratic model for the polarimetric response can be determined and is effective, the stability of solutions over time must still be investigated, and the region of the primary beam under consideration must be extended.

2 Dataset and initial processing

The dataset consists of 17 pointings that are evenly spaced in a cross pattern spanning 1080 arcsec in right ascension and declination, as illustrated in Figure 1. The center pointing, p0, is directed towards the calibrator 3C 286, while the furthest off-center pointing is located at half the distance to the half power point at 3.14GHz. Each of the 17 pointings were scanned 8 times in turn for 50 seconds in each instance. A full 90 degrees range of parallactic angle coverage is attained over a total observing time of $6\frac{1}{2}$ hours, starting at 04h30 on 16 May 2010. Correlations are integrated over 10 seconds. A 100MHz band of 1024 channels is observed, centered at 3.14GHz.

Processing commences with automatic flagging, retaining visibilities from only 28 antennas (1, 3, 4, 7, 8, 11, 12, 13, 15, 17, 19, 23, 24, 25, 26, 27, 28, 29, 30, 31, 32, 33, 34, 35, 36, 39, 40, 41) which each has a 6.1m diameter dish on an alt-az mount. Ten percent of the 100MHz band from both ends of the spectral window are discarded and the remainder is split into 8 segments (about 10MHz per segment) to facilitate a frequency dependent study [Law: 2010]. Calibration is done using Miriad's *mfcal* and *gpcal* tasks, separately for each frequency segment, using only the scans of pointing p0 which is directly towards the calibrator. This calibration determines the bandpass, time varying gain, and leakage solutions per polarization of each antenna. These calibration solutions for pointing p0 are then copied to the off-center pointings, each to its respective frequency segment. The calibration performed up till this point does not include any direction dependent effects, and corrects only for pointing p0.

Thereafter snapshot Stokes I,Q,U,V images are created for each 50 second scan of the observation for all 17 pointings. The Stokes I,Q,U,V values at the source location are extracted from the snapshot images by fitting a point source model using the Mirad task *imfit*. This collection of measured Stokes I,Q,U,V values per pointing per visit is illustrated in Figure 2 where the calibration solution for pointing p0 is applied to all the off-center pointings.

In the figure, the large changes in Stokes I are due to the expected Gaussian sensitivity pattern of the primary beam. Glitches in Stokes I (of unknown cause) are clearly seen in two scans at pointings 5 and 6, and are not removed from the data. More interestingly, errors in Stokes Q and U are noted that seem to change systematically for the off-center pointings. These Stokes Q, U errors seem to be related to Stokes I and have a parallactic angle dependence.

In order to explore the direction dependencies, it is useful to display the scan results on a plane that is stationary with respect to the primary beam, where the effect of parallactic angle rotation has been removed. The right ascension (RA), declination (DEC) coordinates corresponding to the scans can all be mapped to a relative azimuth elevation plane. To calculate the relative azimuth (AZ_{rel}) elevation (EL_{rel}) for a particular off-center scan, the azimuth and elevation coordinates of that scan are subtracted from the azimuth and elevation coordinates of a hypothetical on-center scan (p0) occurring at the same local sidereal time (LST):

$$\begin{aligned}
HA_{p,t} &= LST_t - RA_p \\
\sin(EL_{p,t}) &= \sin(DEC_p)\sin(LAT) + \cos(DEC_p)\cos(LAT)\cos(HA_{p,t}) \\
\tan(AZ_{p,t}) &= \frac{-\sin(HA_{p,t})\cos(DEC_p)}{\sin(DEC_p)\cos(LAT) - \cos(DEC_p)\sin(LAT)\cos(HA_{p,t})} \\
\tan(\chi_{p,t}) &= \frac{\sin(HA_{p,t})\cos(LAT)}{\sin(LAT)\cos(DEC_p) - \sin(DEC_p)\cos(LAT)\cos(HA_{p,t})} \\
EL_{rel,p,t} &= EL_{p,t} - EL_{0,t} \\
AZ_{rel,p,t} &= AZ_{p,t} - AZ_{0,t}
\end{aligned} \tag{1}$$

The time-pointings fill out the plane as illustrated in Figure 3. The same coverage map can be produced by simply rotating the relative right ascension declination pointings around pointing 0 by the average parallactic angle of each scan.

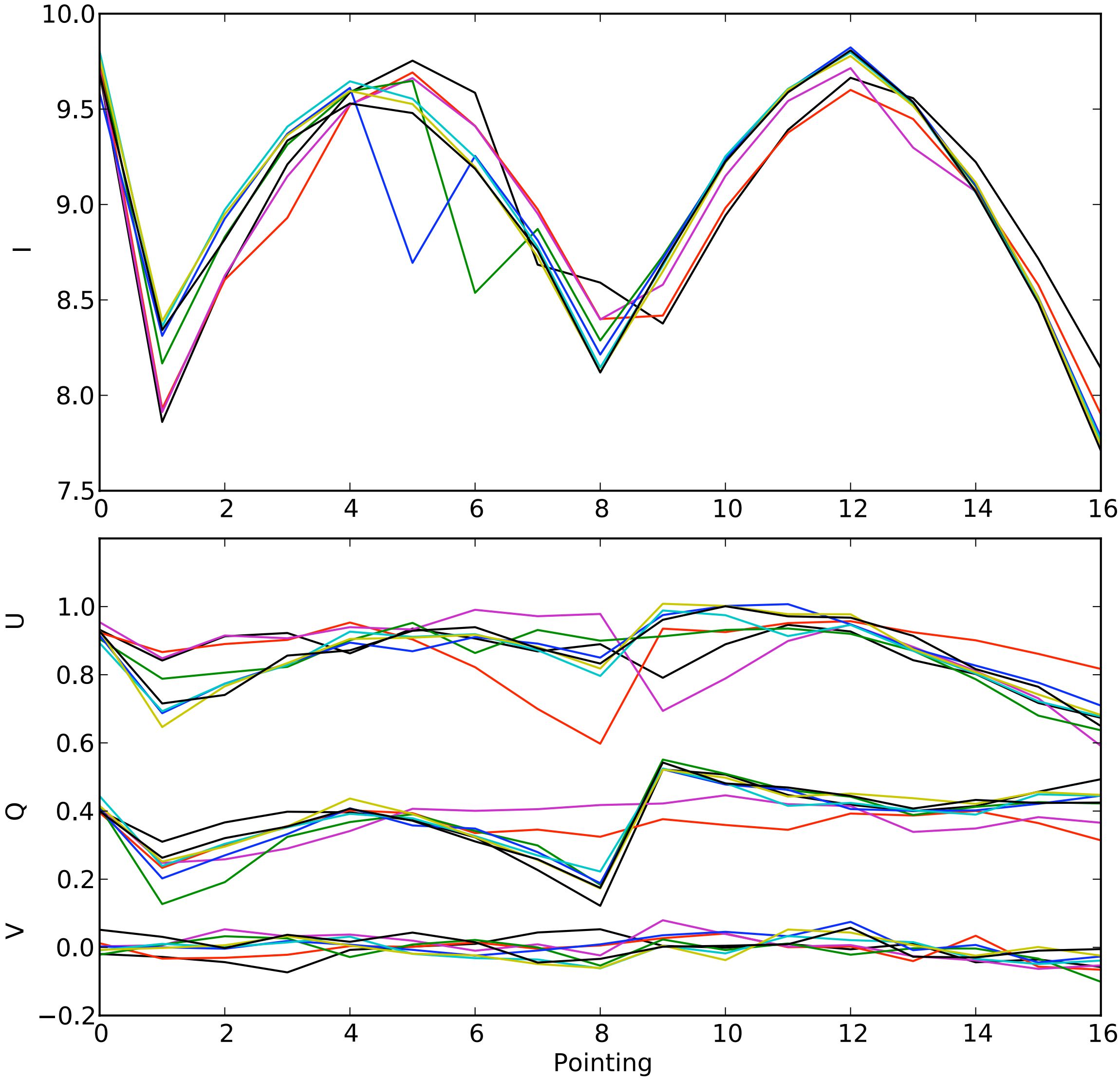

Figure 2: Observed Stokes I,Q,U,V (extracted from snapshot images) are shown for numbered pointings where calibration determined for pointing p0 is applied to all other pointings. Different coloured lines, corresponding to the colours used in Figure 3, are used to distinguish the different times that the same pointings are visited during the observation. Glitches in Stokes I are visible for p5t4 (blue), p6t3 (green) and p7t0 (black). Components of I are notably superimposed onto Q and U as a function of parallactic angle.

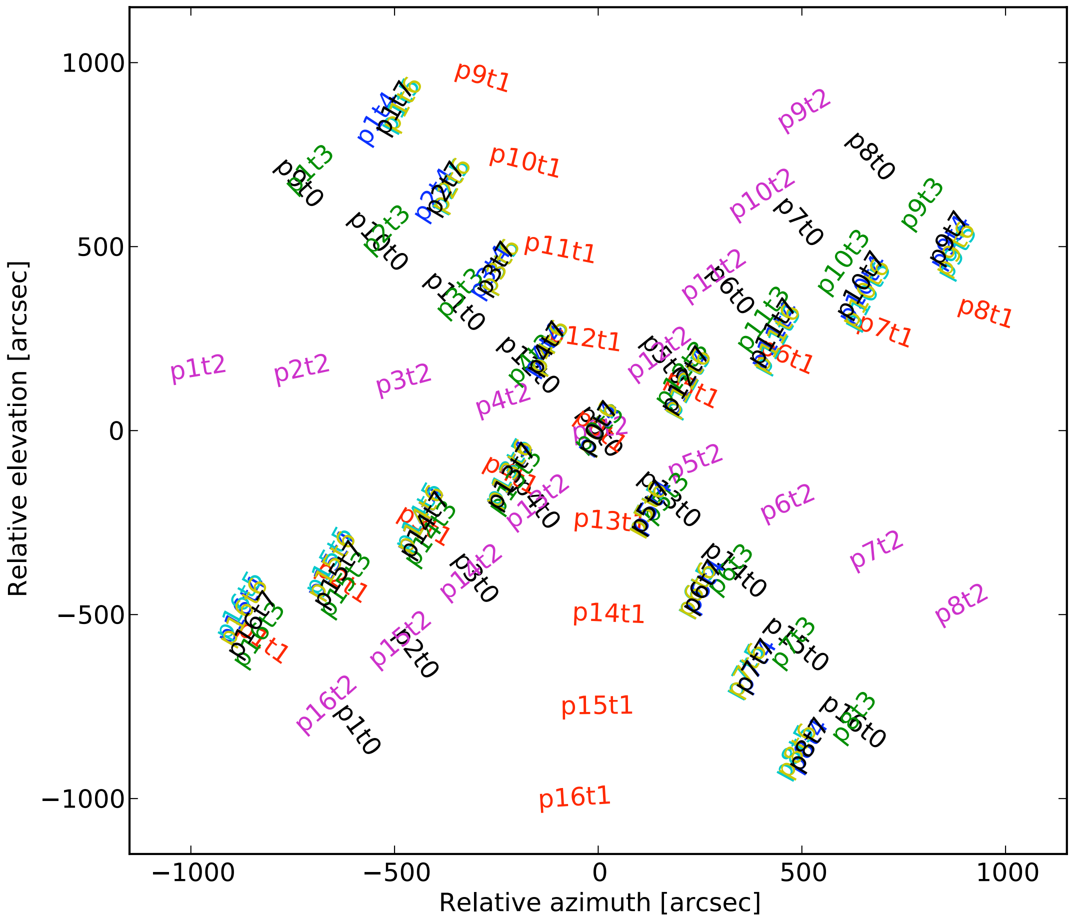

Figure 3: Coverage of the scans relative to the central pointing p0 over the relative azimuth elevation plane for different parallactic angles. The labels are rotated to the parallactic angle of each scan. This plane is stationary with respect to the primary beam. The data points extend out half way to the half power point at 3.14 GHz.

3 Theory

Calibration errors in a radio interferometer will create errors in measured Stokes parameters, $\tilde{s}$. Sault et al. [Sault: 1996] use the matrix equation formalism to derive how relative gain errors and leakage propagate into Stokes errors. To first order, this can be expressed as $\tilde{s} = \mathcal{M}s$ where $s = [IQUV]^{\mathrm{T}}$ is the true Stokes parameters and

$$\mathcal{M}_\chi = \frac{1}{2}\begin{bmatrix} \epsilon_{pp}+2 & -\zeta_{pp}\sin(2\chi)+\epsilon_{np}\cos(2\chi) & \zeta_{pp}\cos(2\chi)+\epsilon_{np}\sin(2\chi) & -\zeta_{nn}j \\ -\zeta_{pp}\sin(2\chi)+\epsilon_{np}\cos(2\chi) & \epsilon_{pp}+2 & \zeta_{np} & \left(-\zeta_{pn}\cos(2\chi)-\epsilon_{nn}\sin(2\chi)\right)j \\ \zeta_{pp}\cos(2\chi)+\epsilon_{np}\sin(2\chi) & -\zeta_{np} & \epsilon_{pp}+2 & \left(-\zeta_{pn}\sin(2\chi)+\epsilon_{nn}\cos(2\chi)\right)j \\ -\zeta_{nn}j & \left(\zeta_{pn}\cos(2\chi)+\epsilon_{nn}\sin(2\chi)\right)j & \left(\zeta_{pn}\sin(2\chi)-\epsilon_{nn}\cos(2\chi)\right)j & \epsilon_{pp}+2 \end{bmatrix} \quad (2)$$

where χ is the parallactic angle. ϵ refers to gain error terms and ζ refers to leakage terms such that

$$\begin{aligned}
\epsilon_{pp} &= \epsilon_{x1} + \epsilon_{y1} + \epsilon^*_{x2} + \epsilon^*_{y2} \\
\epsilon_{nn} &= \epsilon_{x1} - \epsilon_{y1} - \epsilon^*_{x2} + \epsilon^*_{y2} \\
\epsilon_{np} &= \epsilon_{x1} - \epsilon_{y1} + \epsilon^*_{x2} - \epsilon^*_{y2} \\
\zeta_{np} &= D_{x1} - D_{y1} + D^*_{x2} - D^*_{y2} \\
\zeta_{pn} &= D_{x1} + D_{y1} - D^*_{x2} - D^*_{y2} \\
\zeta_{nn} &= D_{x1} - D_{y1} - D^*_{x2} + D^*_{y2} \\
\zeta_{pp} &= D_{x1} + D_{y1} + D^*_{x2} + D^*_{y2}.
\end{aligned} \tag{3}$$

Here, for example, the leakage from the y polarization into the x polarization for antenna 1 is represented by D_{x1}, and the gain, $\tilde{g}_{x1}$, of the x polarization of antenna 1 with respect to the nominal gain is $\tilde{g}_{x1} = g \cdot (1 + \epsilon_{x1})$, following the conventions in [Sault: 1991].

For a single scan of a known source one can regroup the equations and write instead

$$\begin{bmatrix} \tilde{I} \\ \tilde{Q} \\ \tilde{U} \\ \tilde{V} \end{bmatrix} = \begin{bmatrix} I & Q\cos(2\chi) + U\sin(2\chi) & 0 & U\cos(2\chi) - Q\sin(2\chi) & 0 & 0 & -V \\ Q & I\cos(2\chi) & U & -I\sin(2\chi) & -V\sin(2\chi) & -V\cos(2\chi) & 0 \\ U & I\sin(2\chi) & -Q & I\cos(2\chi) & V\cos(2\chi) & -V\sin(2\chi) & 0 \\ V & 0 & 0 & 0 & Q\sin(2\chi) - U\cos(2\chi) & Q\cos(2\chi) + U\sin(2\chi) & -I \end{bmatrix} \begin{bmatrix} \frac{1}{2}\epsilon_{pp} + 1 \\ \frac{1}{2}\epsilon_{np} \\ \frac{1}{2}\zeta_{np} \\ \frac{1}{2}\zeta_{pp} \\ j\frac{1}{2}\epsilon_{nn} \\ j\frac{1}{2}\zeta_{pn} \\ j\frac{1}{2}\zeta_{nn} \end{bmatrix}. \tag{4}$$

This equation suggests that the observed Stokes I,Q,U,V, combined with the known Stokes I,Q,U,V and parallactic angle can be used to solve for the mean leakage, ζ, and gain errors, ϵ, by matrix inversion. Note that there are seven ϵ and ζ parameters to solve for but only four Stokes parameters and the parallactic angle are known. Uniquely solving for the ζ, ϵ values requires us to either model them or use values from multiple scans.

Observed Stokes I,Q,U,V data, the parallactic angle, and the true Stokes I,Q,U,V values of the source is indeed available over the relative azimuth elevation plane illustrated in Figure 3. If data is combined within a neighbourhood, it is possible to solve for the seven ϵ, ζ parameters within such a neighbourhood, at any point in the plane. Such a neighbourhood can easily be implemented in the matrix formulation by including all the data over the plane, whilst weighing the equations due to the i-th scan based on the distance from the point of interest (AZ_{rel}, EL_{rel}) to the location of the i-th scan in the relative azimuth elevation plane, using a Gaussian footprint:

$$w_i(AZ_{rel}, EL_{rel}) = \exp\left[-\frac{1}{2}\frac{(AZ_{rel,i} - AZ_{rel})^2 + (EL_{rel,i} - EL_{rel})^2}{\sigma^2}\right]. \tag{5}$$

Implementing such a neighbourhood directly does unfortunately convolve the solution by the neighbourhood footprint. To overcome this issue, instead of solving for ϵ and ζ values directly, one can solve for a model that describes the ϵ and ζ surfaces within such a neighbourhood. By examining solutions solved within a neighbourhood without imposing a model (not shown), it appears that a quadratic would be a suitable parameterization for ϵ ζ maps over the part of the primary beam being investigated. ζ_{pn} and ϵ_{nn} are however modeled using a constant over the neighbourhood instead. This is done because the data seem to constrain ζ_{pn} and ϵ_{nn} only weakly, and using a quadratic here results in overfitting.

Once the parameterized ϵ, ζ maps are determined, ϵ, ζ values can be calculated at any point in the field and be used to predict true Stokes I,Q,U,V values from observed Stokes I,Q,U,V values using $s = \mathcal{M}_\chi^{-1}\tilde{s}$ which also requires knowledge of the parallactic angle. Processing in this way would necessitate imaging in snapshot mode, unless the polarimetric model is used in an A-projection algorithm [Rau: 2009] although this option is presently not available in Miriad.

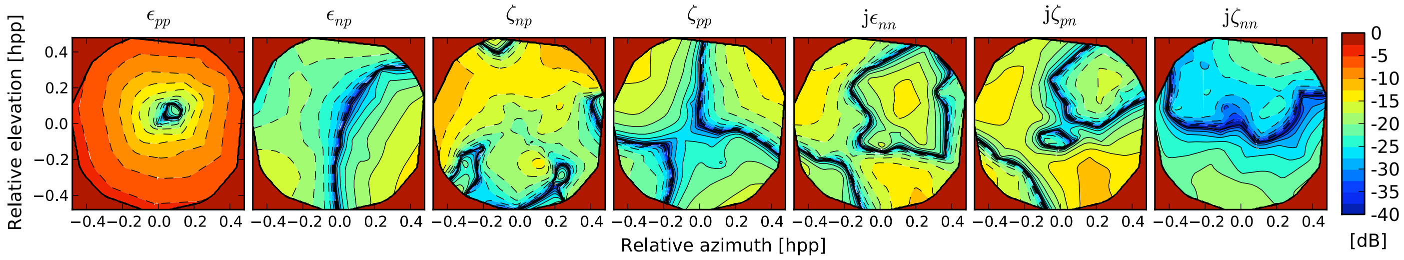

(a) $\sigma = 0.5$ ***hpp***

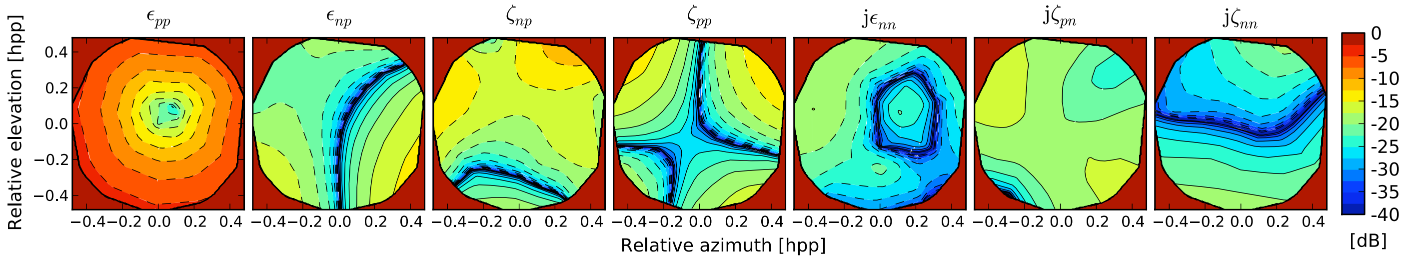

(b) $\sigma = 1$ ***hpp***

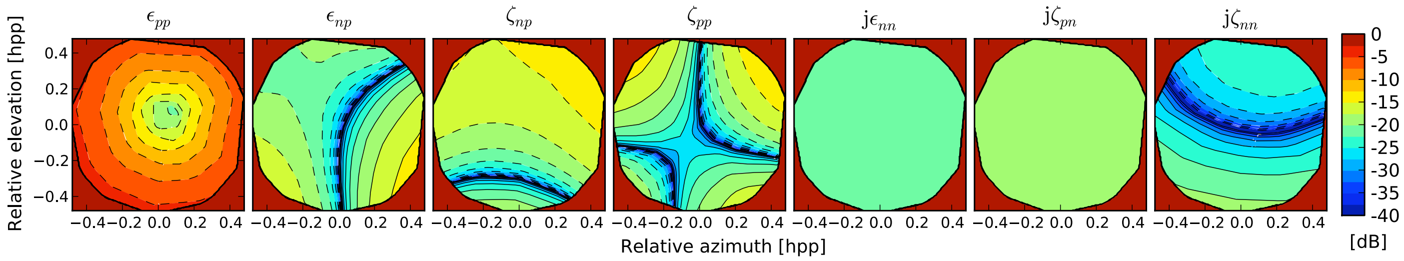

(c) $\sigma = 10$ ***hpp***

Figure 4: ϵ, ζ maps constrained in a neighbourhood to a quadratic model for a range of neighbourhood sizes. Because values are only evaluated at the datapoints and are otherwise linearly interpolated for display, the images (especially ϵ_{pp}) appear more jaggered than they should be. The distance to the half power point (hpp) is 2160 arcseconds. Dashed contours indicate negative values. Model name: qqqqccq. The characters q (quadratic) and c (constant) in the model name refer to the models used for the respective seven ϵ, ζ components.

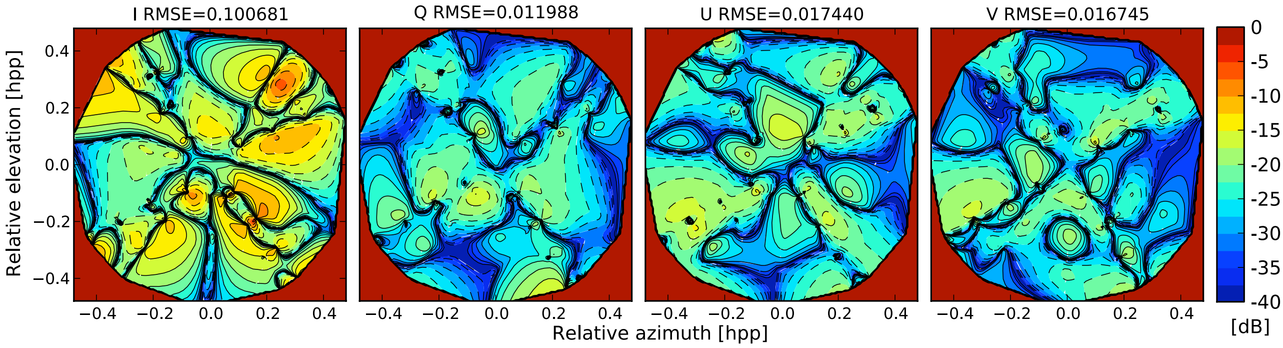

(a) $\sigma = 0.5$ ***hpp***

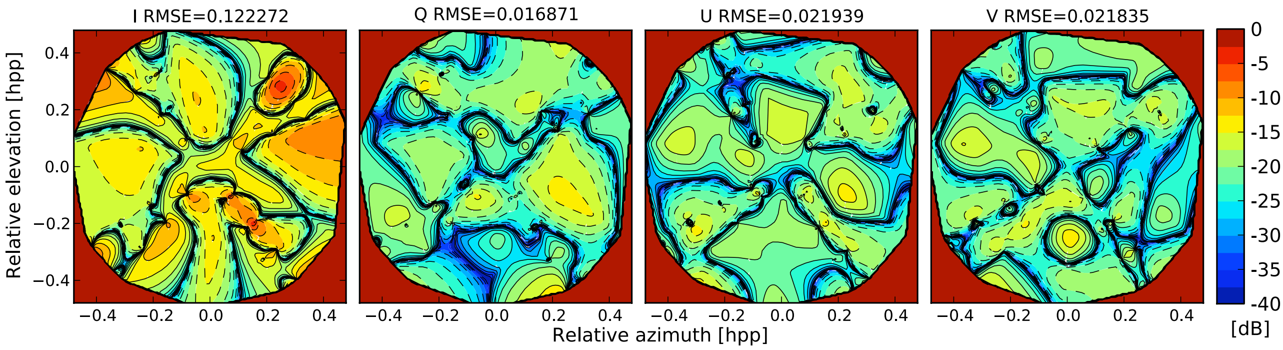

(b) $\sigma = 1$ ***hpp***

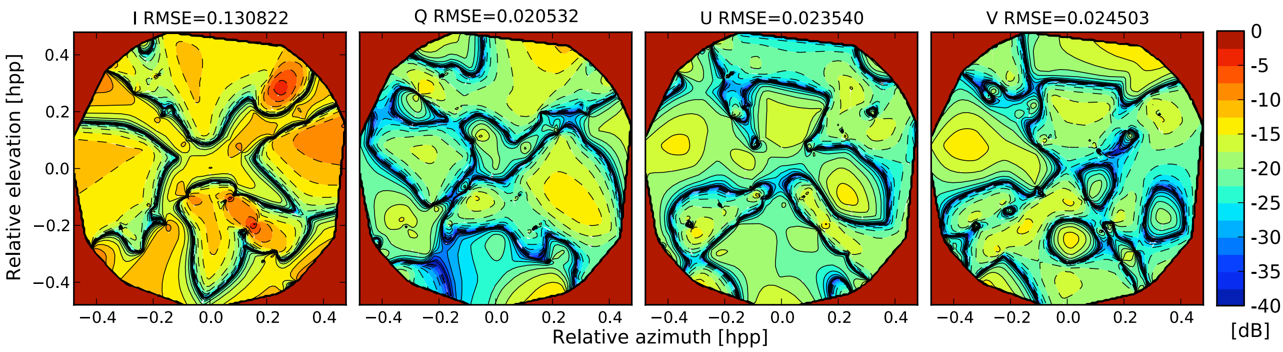

(c) $\sigma = 10$ ***hpp***

Figure 5: Remaining error over the field. The figure shows the difference between the predicted and true Stokes values for off-center observations of the calibrator source 3C 286. The distance to the half power point (hpp) is 2160 arcseconds. Dashed contours indicate negative values. Model name: qqqqccq

4 Results

Figure 4 shows results for solutions to the ϵ, ζ maps using quadratic models for ϵ_{pp}, ϵ_{np}, ζ_{np}, ζ_{pp} and ζ_{nn}, and constants for ϵ_{nn} and ζ_{pn}. Separate solutions are found within a neighbourhood for each point in the relative azimuth elevation plane. Therefore, only when the Gaussian weighted neighbourhood encompasses the entire plane with equal weighting to equations from all scans (this happens when σ=10 times the distance to the half power point, which is 21600 arcseconds) are the solutions constrained to be quadratic functions or constants across the field. For smaller values of σ, piecewise quadratic (or constant) solutions are calculated.

If the model-predicted Stokes I,Q,U,V is subtracted from the true Stokes I,Q,U,V for the observations of calibrator 3C 286, the remaining error over the field is shown in Figure 5. Figure 6 shows this result in a form comparable to Figure 2. RMS errors of down to 1.35% in I, 0.21% in Q, 0.24% in U and 0.25% in V (for one minute observations of 3C 286) is achieved compared to the true Stokes I for off-center pointings across the primary beam up to half the distance to the half power point. Note that the RMS error in Stokes I dramatically reduces to 0.75% if the three glitches seen clearly in Figure 6 are removed.

For reference, the RMS errors of the on-axis scans (of pointing p0, directly towards the calibrator source) alone, are 0.67% in I, 0.14% in Q, 0.18% in U and 0.22% in V when traditional calibration at the phase center is performed. These errors are representative of the dynamic range and thermal noise limit, and prevail because the duration of each scan is merely a minute. For a science target observation, better results are expected when time synthesis is employed.

Figure 7 shows results where ϵ_{np}, ζ_{np}, ζ_{pp}, ζ_{nn}, ϵ_{nn} and ζ_{pn} are modeled using constants (while ϵ_{pp} is modeled by a quadratic) which is equivalent to the case of not correcting for direction dependent effects other than normalizing by the primary beam power pattern. In this case the RMS errors are 1.37% in I, 0.96% in Q, 0.88% in U and 0.36% in V compared to the true Stokes I value.

The abovementioned results are listed more comprehensively as absolute errors in Table 1, and repeated as errors relative to the true Stokes I in Table 2. In these tables the model name is composed of characters *q* (for quadratic) and *c* (for constant) which signify the type of model used for the respective maps ϵ_{pp}, ϵ_{np}, ζ_{np}, ζ_{pp}, ϵ_{nn}, ζ_{pn} and ζ_{nn}. The models are solved within a neighbourhood of size specified by σ in units of the fraction of the distance to the half power point. Table 3 provides the fitted coefficient values that describe the ϵ, ζ maps over the relative azimuth elevation plane for the model qqqqccq, σ=10.

5 Conclusion

We present a technique that uses observed Stokes I,Q,U,V errors to derive direction dependent leakage and gain errors for a radio interferometer. It is shown that a simple quadratic model for direction dependent gain error and leakages can be inferred from pointings nearby to a known calibrator source. The results show that such a model can be used to predict corrections to imaged Stokes I,Q,U,V values as a function of parallactic angle. This is demonstrated with observations of 3C 286 using the ATA at 3.14GHz.

The method shows improvements in RMS errors for Stokes I,Q,U,V across the field, which in this study was up to half the distance to the half power point. Without direction dependent corrections, the RMS errors are 1.37% in I, 0.96% in Q, 0.88% in U and 0.36% in V compared to the true Stokes I. When the simple quadratic model is employed, the RMS errors become 1.35% in I, 0.21% in Q, 0.24% in U and 0.25% in V across the field, which for Q, U and V are similar to typical on-axis image quality. Poor results for Stokes I are due to glitches that are not removed from the data. Better results are possible if piecewise quadratic models are used.

Model	$I_{\max\|E\|}$	$Q_{\max\|E\|}$	$U_{\max\|E\|}$	$V_{\max\|E\|}$	I_{RMSE}	Q_{RMSE}	U_{RMSE}	V_{RMSE}
qqqqccq, $\sigma = 0.5$	0.74	0.035	0.065	0.053	0.10	0.012	0.017	0.017
qqqqccq, $\sigma = 1$	0.84	0.049	0.072	0.074	0.12	0.017	0.022	0.022
qqqqccq, $\sigma = 10$	0.87	0.068	0.075	0.075	0.13	0.020	0.024	0.025
qcccccc, $\sigma = 10$	0.87	0.258	0.254	0.122	0.13	0.093	0.086	0.035
none	2.01	0.289	0.331	0.103	0.91	0.093	0.111	0.032
none, on-axis	0.14	0.033	0.032	0.050	0.07	0.014	0.017	0.022

Table 1: Absolute errors in Stokes I,Q,U,V measured across the field. For reference, values in the last row are derived from on-axis scans (of pointing p0) only.

Model	$I_{\max\|E\|}$	$Q_{\max\|E\|}$	$U_{\max\|E\|}$	$V_{\max\|E\|}$	I_{RMSE}	Q_{RMSE}	U_{RMSE}	V_{RMSE}
qqqqccq, $\sigma = 0.5$	7.6%	0.36%	0.67%	0.55%	1.04%	0.12%	0.18%	0.17%
qqqqccq, $\sigma = 1$	8.7%	0.50%	0.74%	0.77%	1.26%	0.17%	0.23%	0.22%
qqqqccq, $\sigma = 10$	8.9%	0.70%	0.77%	0.77%	1.35%	0.21%	0.24%	0.25%
qcccccc, $\sigma = 10$	8.9%	2.65%	2.61%	1.25%	1.37%	0.96%	0.88%	0.36%
none	20.7%	2.97%	3.41%	1.06%	9.39%	0.96%	1.15%	0.33%
none, on-axis	1.42%	0.34%	0.33%	0.52%	0.67%	0.14%	0.18%	0.22%

Table 2: Errors in Stokes I,Q,U,V measured across the field, expressed as a percentage of the true Stokes I. For reference, values in the last row are derived from on-axis scans only.

Map	a_0	a_1	a_2	a_3	a_4	a_5
$\frac{1}{2}\epsilon_{pp} + 1$	-5.92965136e-01	6.02962732e-02	-9.21986156e-03	6.62856253e-02	-5.89025251e-01	9.94065099e-01
$\frac{1}{2}\epsilon_{np}$	2.15877513e-02	2.49413754e-02	-5.94928838e-02	-6.62384725e-03	-1.48096116e-02	-7.00064176e-04
$\frac{1}{2}\zeta_{np}$	-2.72813204e-02	-7.42125016e-03	1.53955964e-03	-2.44480828e-02	2.06533842e-02	-9.10807742e-03
$\frac{1}{2}\zeta_{pp}$	-1.71157605e-02	-1.83882334e-02	-1.21946981e-01	-5.06502783e-03	1.29041887e-02	2.72060584e-04
$\mathrm{j}\frac{1}{2}\epsilon_{nn}$	0	0	0	0	0	-3.42902092e-03
$\mathrm{j}\frac{1}{2}\zeta_{pn}$	0	0	0	0	0	6.65407653e-03
$\mathrm{j}\frac{1}{2}\zeta_{nn}$	5.62279585e-03	-1.85949822e-03	-7.80202503e-04	-8.81762897e-03	8.58295590e-03	-2.54849430e-04

Table 3: Fitted coefficient values that describe the ϵ, ζ maps over the relative azimuth elevation plane for model qqqqccq, σ=10. Here the respective ϵ, ζ maps$(AZ_{rel}, EL_{rel}) = a_0 AZ_{rel}^2 + a_1 AZ_{rel} + a_2 AZ_{rel} EL_{rel} + a_3 EL_{rel} + a_4 EL_{rel}^2 + a_5$ where the units for AZ_{rel}, EL_{rel} is the fraction of the distance to the half power point.

6 Recommendations

A further observation is needed to test the inferred model on data with polarization properties different to that of the calibrator. Such a new dataset could also be used to test for stability over time of the direction dependent maps, and form the basis of a study for a more refined observation and calibration strategy. We also still need to investigate how applicable the quadratic model is up to the half power point of the primary beam.

7 Acknowledgements

Thanks to Geoffrey Bower, Jasper Horrell, Debra Sheperd, Ludwig Schwardt, the Berkeley MMM group and SKA SA.

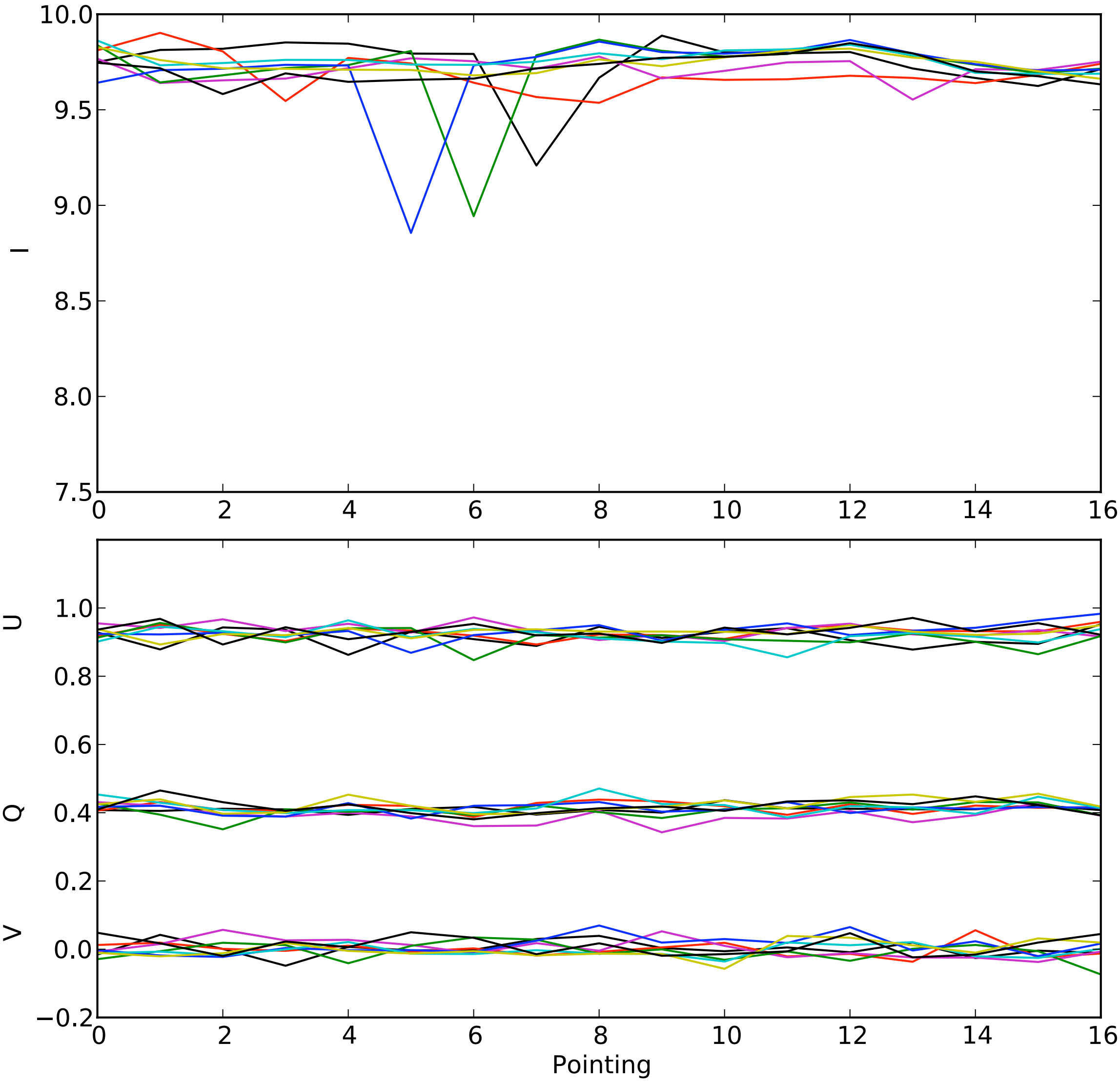

Figure 6: Predicted Stokes I,Q,U,V values for the various scans using models for ϵ_{pp}, ϵ_{np}, ζ_{np}, ζ_{pp} and ζ_{nn} that are quadratic and models for ϵ_{nn}, ζ_{pn} that are constant over the primary beam. Compare to Figure 2. The glitches in Stokes I remain, and seem to be due to suspicious data. RMS errors of 1.35% in I, 0.21% in Q, 0.24% in U and 0.25% in V are calculated as a percentage of the true Stokes I for 3C 286. Model name: qqqqccq, σ=10.

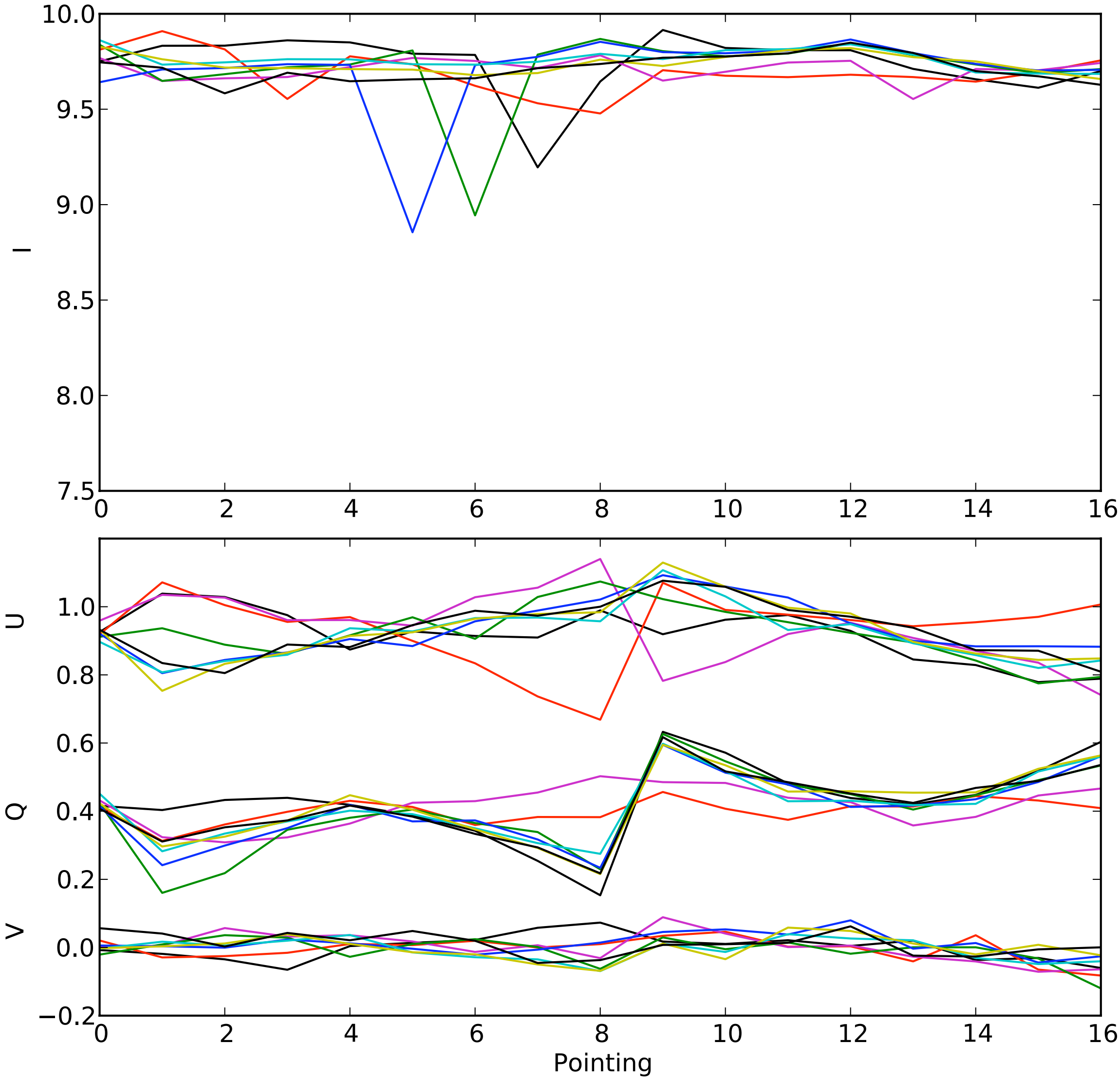

Figure 7: Predicted Stokes I,Q,U,V values for the various scans using a model for ϵ_{pp} that is quadratic and models for ϵ_{np}, ϵ_{nn}, ζ_{pp}, ζ_{np}, ζ_{pn} and ζ_{nn} that are constants over the primary beam. RMS errors of 1.37% in I, 0.96% in Q, 0.88% in U and 0.36% in V are calculated as a percentage of the true Stokes I for 3C 286. Model name: qcccccc, σ=10.

References

[Bhatnagar: 2008] Bhatnagar et al. Correcting direction-dependent gains in the deconvolution of radio interferometric images. A&A 487, 419-429, 2008.

[Rau: 2009] U. Rau, S. Bhatnagar, M. A. Voronkov,T. J. Cornwell. Advances in Calibration and Imaging Techniques in Radio Interferometry. Proceedings of the IEEE, Vol.97, No.8, p-1472, August 2009.

[Law: 2010] C. Law, M. de Villiers. On-axis Polarization Calibration with the ATA. ATA Technical memo series. October, 2010.

[Sault: 1991] Sault et al. AT Polarisation Calibration. AT Memo series. September 19, 1991.

[Sault: 1996] Sault et al. Understanding radio polarimetry. II. A&A 117, 149-159, 1996.